Mon. Not. R. Astron. Soc. **308**, 939–946 (1999)

The kinematics of NGC 4361, a Population II planetary nebula with a bipolar outflow

R. Vázquez,[1,2]★ J. A. López,[2] L. F. Miranda,[1] J. M. Torrelles[3,1] and J. Meaburn[4]

[1]*Instituto de Astrofísica de Andalucía, CSIC, Apdo. Postal 3004, 18080 Granada, Spain*
[2]*Instituto de Astronomía, UNAM, Apdo. Postal 877, 22800 Ensenada, B.C., Mexico*
[3]*Institut d'Estudis Espacials de Catalunya (IEEC/CSIC), Edifici Nexus, C/Gran Capitá 2-4, E-08034 Barcelona, Spain*
[4]*Department of Physics and Astronomy, University of Manchester, Oxford Road, Manchester M13 9PL*

Accepted 1999 April 8. Received 1999 March 29; in original form 1999 January 22

ABSTRACT

High-resolution, spatially-resolved profiles of Hα, He II λ6560 and [O III] λ5007 and deep narrow-band CCD images in the Hα and [O III] λ5007 emission lines have been obtained of the planetary nebula (PN) NGC 4361. In addition, VLA-DnC λ3.6-cm continuum observations are presented. This material allows one to explore in unprecedented detail the morphology and kinematics of this PN. The morphology of this object is complex given the highly filamentary structure of the envelope, which is confirmed to possess a low mass. The halo has a high expansion velocity that yields incompatible kinematic and evolutionary ages, unless previous acceleration of the nebular expansion is considered. However, the most remarkable result from the present observations is the detection of a bipolar outflow in NGC 4361, which is unexpected in a PN with a Population II low-mass-core progenitor. It is shown that shocks resulting from the interaction of the bipolar outflow with the outer shell are able to provide an additional heating source in this nebula.

Key words: ISM: abundances – ISM: kinematics and dynamics – planetary nebulae: individual: NGC 4361 – ISM: structure.

1 INTRODUCTION

NGC 4361 is a very-high-excitation planetary nebula (PN), which, according to Torres-Peimbert, Peimbert & Peña (1990, hereafter TPPP), must be a Population II object given its chemical abundances (with heavy element deficiencies implying a small core mass), its distance to the Galactic plane (0.83 kpc) and the low mass of its nebular envelope. Peimbert (1990) has accordingly classified it as a type IV PN.

The global morphology of NGC 4361 is apparent in the ESO/SERC Southern Sky Atlas *R* band given in Chu, Arendt & Jacoby (1987), in which a bright inner and a more extended outer shell or halo can be discerned. In addition, Chu & Jacoby (1987) have pointed out that the outer shell expands faster than the inner shell. The only published kinematic information on NGC 4361, however, seems to be the data by Meatheringham, Wood & Faulkner (1988), who derive an [O III] expansion velocity $V_{\rm exp} = 25.8\,{\rm km\,s^{-1}}$, presumably from the central bright region of the nebula. The inner structure of NGC 4361 can be partially discerned also in images published by Schwarz, Corradi & Melnick (1992). Curious point-symmetric-like extensions are seen to emerge from the central region and in opposite directions along PA $\approx$ 45°, which give a 'spiral' looking structure to the inner nebula.

Recently, Liu (1998) has pointed out the presence of substantial temperature variations ($\pm$1000 K) across the nebula and suggests that these are probably produced by shock heating. Low velocity shocks have been shown before to play an important role in filamentary halos of some planetary nebulae (PNe), such as NGC 6543 (Bryce et al. 1992).

These peculiar characteristics have driven us to obtain additional data for a better inspection of the morphology of NGC 4361 and its kinematics.

2 OBSERVATIONS AND RESULTS

2.1 CCD narrow-band imagery

Deep narrow-band images of NGC 4361 in the light of Hα (10-Å HPBW) and [O III] λ5007 (60-Å HPBW) were obtained in 1997 May 3 with the 1.5-m (f/13.5) San Pedro Mártir UNAM telescope. Exposure times were 1800 and 1200 s, respectively. A Tektronix CCD with 1024×1024, 24-μm (0.257-arcsec) square pixels was the detector. 'Seeing' varied between 1 and 2 arcsec during these observations. Images were reduced in the standard manner using IRAF. These are shown in Fig. 1. The [O III] image has also been

★ E-mail: vazquez@bufadora.astrosen.unam.mx

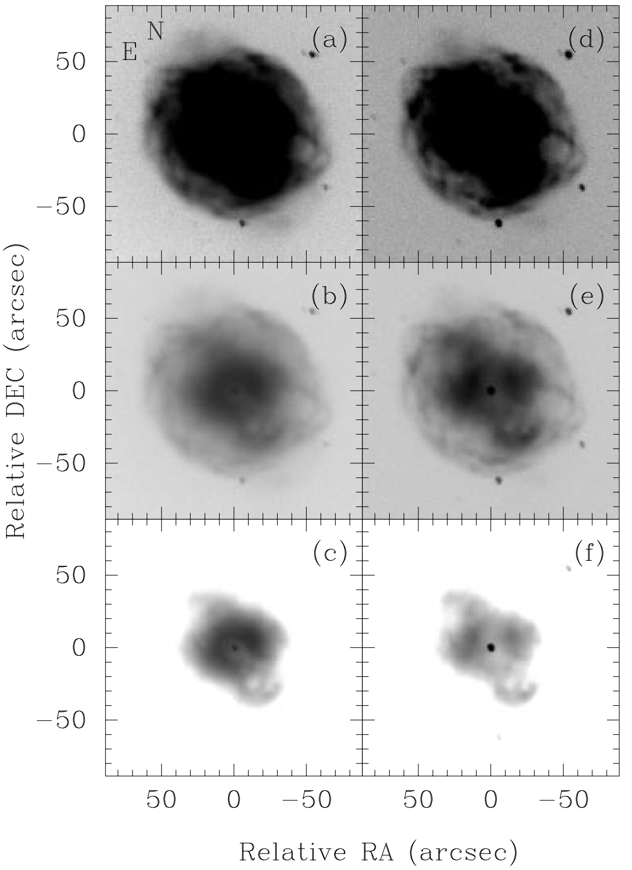

Figure 1. Logarithmic negative representations of the images of NGC 4361 in the light of Hα (a, b, c) and [O III] λ5007 (d, e, f). In both cases, levels are arbitrarily chosen to reveal diferent aspects of the morphology. North is top and East is left.

processed with an unsharp masking filter that allows one to discern the highly filamentary structure of the nebula; this is shown in Fig. 2.

2.2 Long-slit echelle spectroscopy

The long-slit spectral observations were obtained with the Manchester Echelle Spectrometer (MES; Meaburn et al. 1984) combined with the f/7.9 focus of the 2.1-m San Pedro Mártir UNAM telescope during 1996 April 16 and 17. This spectrometer has no cross-dispersion. The same Tektronix CCD was used, on this occasion with a frame scale of $\equiv 0.3$ arcsec pixel^{-1}. Two-times binning was employed in both spatial and spectral dimensions. Consequently 512 increments, each 0.60-arcsec long, gave a total projected slit length of 5.12 arcmin on the sky. Data reduction and wavelength calibration were performed using the standard techniques with IRAF. The spectra were calibrated to ± 1 km s^{-1} accuracy against that of a Th–Ar arc lamp. The slit was always oriented E–W with integration times ranging from 1200 to 1800 s.

Two sets of long-slit spectral observations were made. In the first one, a filter of 90-Å bandwidth was used to isolate the 87th order containing the Hα and He II λ6560 lines (the [N II] $\lambda\lambda$6548, 6584 nebular emission lines are practically absent in this very-high-excitation nebula, in which most ions are in high-ionization stages). The single slit was 150-μm wide ($\equiv 12$ km s^{-1} and 1.9 arcsec). For the second set, the same slit with a 70-Å bandwidth filter isolating the [O III] λ5007 line in the 114th order was used ($\equiv 13$ km s^{-1}). The slit positions, marked A to E, are shown in Fig. 3 against an [O III] contour map/grey-scale of the nebula. The first set comprises slit positions C and E, whereas the second set includes slit positions A to D. The offsets with respect to the central star (relative declination set to zero) are: +47 arcsec (slit A), +21 arcsec (slit B), +4 arcsec (slit C), −17 arcsec (slit D) and −25 arcsec (slit E). These positions are particularly well known because a plane mirror can be inserted into the beam

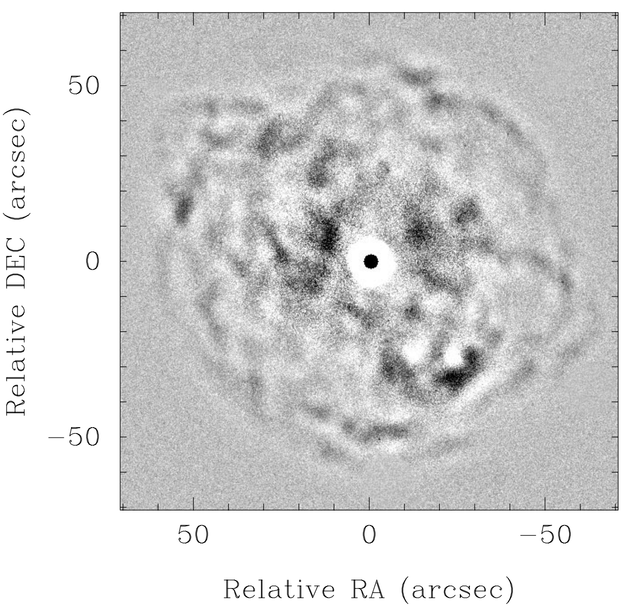

Figure 2. The [O III] image of NGC 4361 after processing with an unsharp masking filter that highlights the filamentary structure of the nebula.

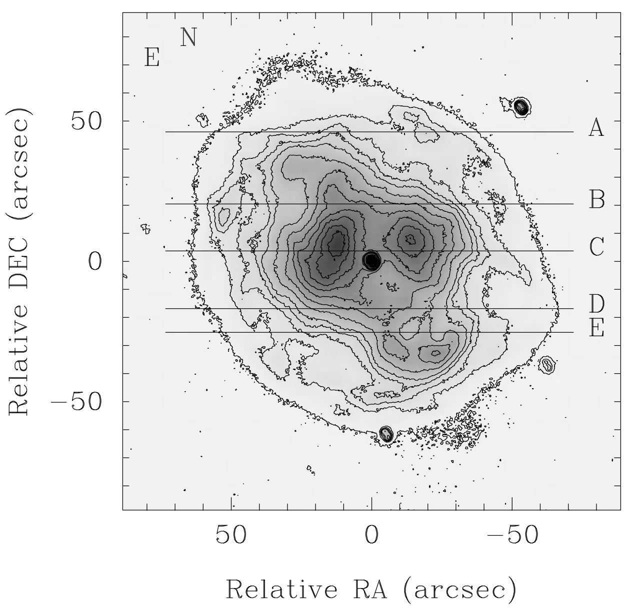

Figure 3. MES slit positions A to E are marked against an [O III] contour map/grey-scale of NGC 4361.

before the echelle grating of the MES, permitting an image to be taken of the slit against that of the field being observed.

Contour-plot/grey-scale representations of the resulting position–velocity (PV) arrays of the Hα and He II λ6560 profiles for slit positions C and E are shown in Fig. 4. The corresponding [O III] λ5007 profiles for slit positions A to D are shown in Figs 5 and 6. The spatial extent in these figures corresponds to the length of the slits marked in Fig. 3.

2.3 λ3.6-cm radio continuum

The λ3.6-cm continuum observations were made with the VLA of the National Radio Astronomy Observatory (NRAO) in the DnC configuration during 1996 May 16. (The National Radio Astronomy Observatory is a facility of the National Science Foundation operated under cooperative agreement by Associated Universities Inc.) The standard VLA continuum mode with a bandwidth of 100 MHz and two circular polarizations was employed. The absolute flux calibrator was 3C 286 (adopted flux density 5.3 Jy at λ3.6 cm), while 1239–103 was used as phase calibrator (observed flux density 1.2 Jy at λ3.6 cm). Phase centre was set in $\alpha(2000) = 12^h24^m31^s$, $\delta(2000) = -18°47'09''$. The on-target integration time was 28 min. The data were calibrated and processed using standard procedures of the AIPS package of the NRAO. A cleaned map of NGC 4361 was obtained using the task MX of AIPS with a uniform weight for the *uv* data. The resulting synthesized beam is $21.1 \times 7.0\,\mathrm{arcsec}^2$ (PA $-54°$), while the rms noise of the map $\sigma = 80\,\mu\mathrm{Jy\,beam}^{-1}$. A contour map/grey-scale of the resulting map is shown in Fig. 7.

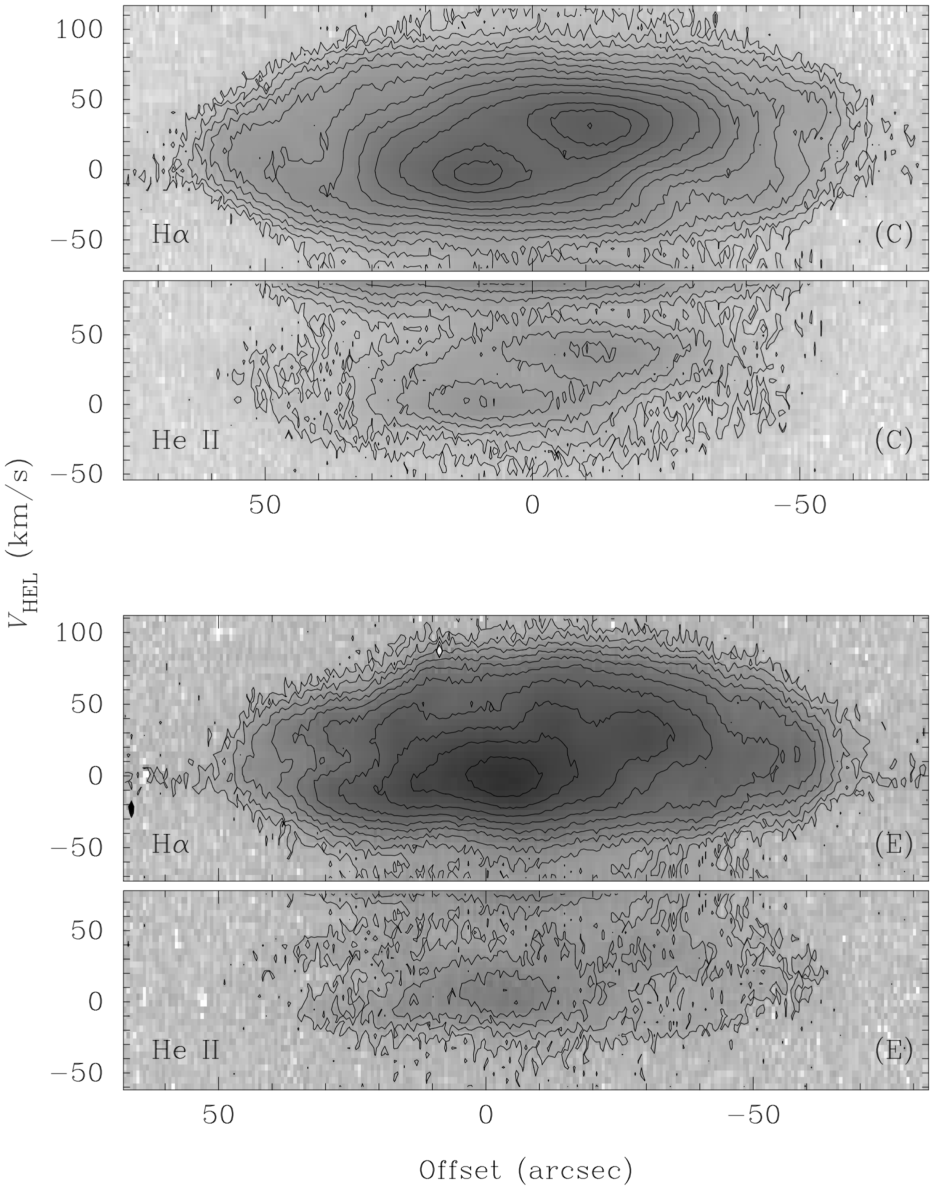

Figure 4. Negative grey-scale representations with contours overplotted of the position–velocity arrays of the Hα and He II λ6560 line profiles for slit positions C and E. Spatial extent is as shown in Fig. 3.

3 DISCUSSION

3.1 Morphology

The images in Figs 1, 2 and 3 show an extended filamentary halo ≈ 110 arcsec in diameter. The bright inner (≈ 60 arcsec) region has an elliptical appearance in the saturated images and is in fact dominated by two bright [O III] clumps located on opposite sides (E–W) of the central star. A pair of prominent filaments seemingly emerge from the inner region, in nearly perpendicular directions to the plane defined by the bright [O III] clumps and they appear to be bent in opposite directions, resembling point-symmetric extensions, giving to this inner region a 'spiral' looking shape. The morphology of this object is complex given the highly filamentary structure of the envelope, which is dramatically revealed in the [O III] unsharp masked image in Fig. 2. The unsharp masking filter retains the high spatial frequencies in the image, highlighting clumps, knots and filaments that are otherwise swamped by the diffuse emission.

3.2 The ionized mass of the envelope

The λ3.6-cm continuum map in Fig. 7 shows the general features present in the optical images. The peak flux density of the map is $S_{\rm peak} = 8.9\,{\rm mJy\,beam^{-1}}$ and the total flux density is $S_{\rm total} = 120\,{\rm mJy}$. Following the formulation by Mezger & Henderson (1967) for optically-thin free–free emission, a mean electron density $N_{\rm e} = 220\,{\rm cm^{-3}}$ and an ionized mass for the envelope $M({\rm H\,II}) = 0.4\,{\rm M_\odot}$ are obtained. An electron temperature of 1.8×10^4 K (TPPP; Liu 1998), a distance $d = 1.2$ kpc (Méndez et al. 1988), and an HPW for the flux density distribution $\theta = 55$ arcsec have been adopted. However, the radio continuum emission in NGC 4361 should mainly come from the high-density

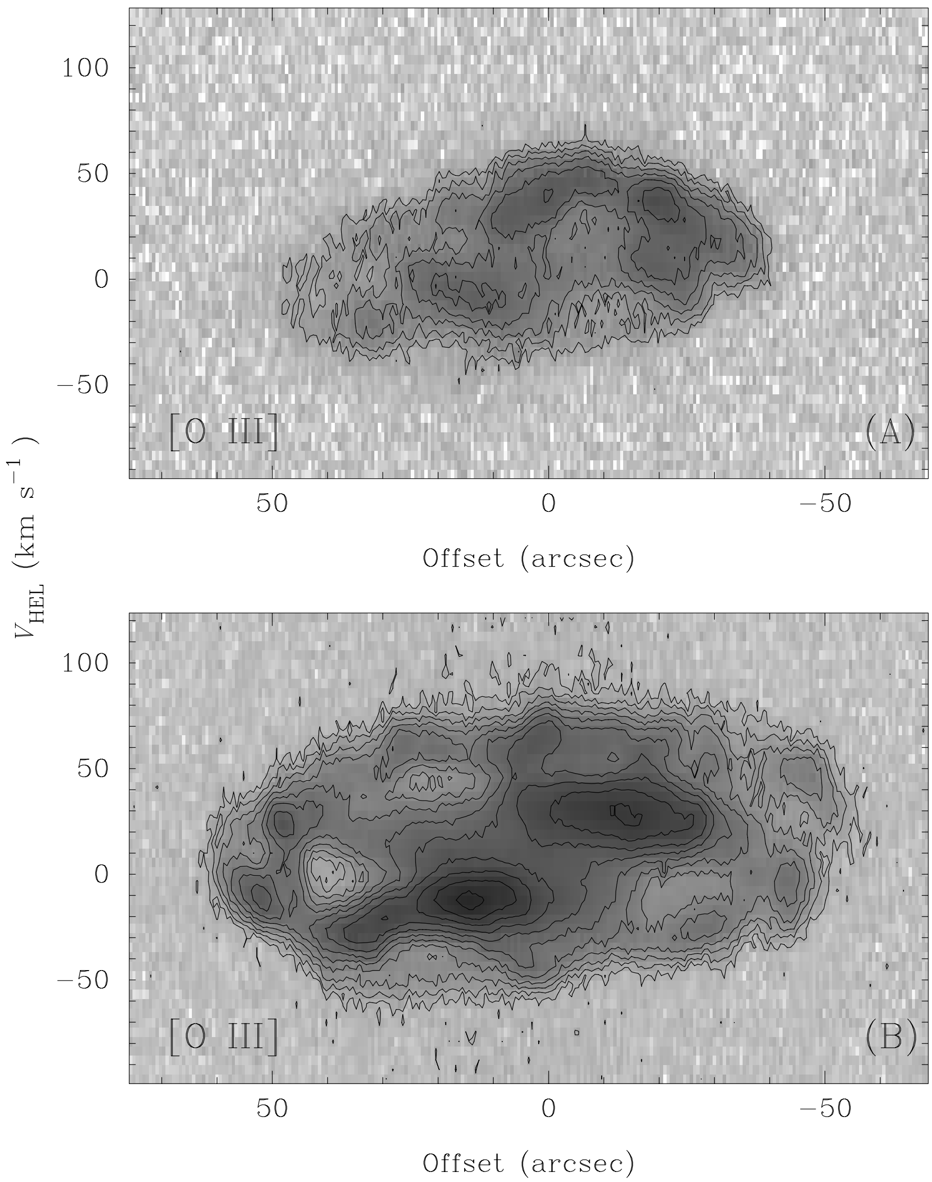

Figure 5. As Fig. 4 but for the position–velocity arrays of the [O III] λ5007 line profiles for slit positions A and B.

clumps and filaments seen in the optical images (see Figs 1 and 2), therefore a volume filling factor needs to be considered for a proper evaluation of the ionized mass. A volume filling factor has been derived from the present rms electron density and the value derived by Liu (1998) from the [Ar IV] forbidden lines (FL) that trace the local electron density from the highest density regions in the nebula, $N_e(\mathrm{FL}) = 1200\,\mathrm{cm}^{-3}$, i.e. $\epsilon = N_e(\mathrm{rms})^2/N_e(\mathrm{FL})^2 = 0.0333$ (see TPPP). Thus, a more realistic value of the ionized mass for the envelope is $M(\mathrm{H\,II}) = \epsilon^{1/2}\ M(\mathrm{H\,II})_{\mathrm{rms}} = 0.07\,\mathrm{M}_\odot$

This result is in agreement with the corresponding one derived in TPPP, supporting their assertion of a low mass for the nebular envelope.

3.3 Kinematics

The long-slit profiles in Figs 4, 5 and 6 show distinct velocity ellipses corresponding to the extended, expanding halo and in addition complex inner structures that do not correspond to the expected kinematic behaviour of a simple radially expanding inner shell. The morphology of NGC 4361 is now inspected considering the peculiar structure of the line profiles.

3.3.1 The halo

The top panels in Figs 4 and 6 correspond to the long-slit position C for the Hα and [O III] line profiles that cross the nebula through its centre (see Fig. 3). At this position, the expansion of the outer shell reaches its maximum values, with $V_{\mathrm{exp}} = 70\,\mathrm{km\,s^{-1}}$ (+90 and $-50\,\mathrm{km\,s^{-1}}$). This is a very high expansion velocity for a halo. Furthermore, this halo is not expanding in a spherically symmetric way. In all the line profiles in Figs 4 to 6 it can be clearly discerned that the radial velocity towards which the halo converges shows a well-defined tilt. The apex of the velocity ellipse terminates at $V_{\mathrm{HEL}} \simeq 0\,\mathrm{km\,s^{-1}}$ on the eastern side but at

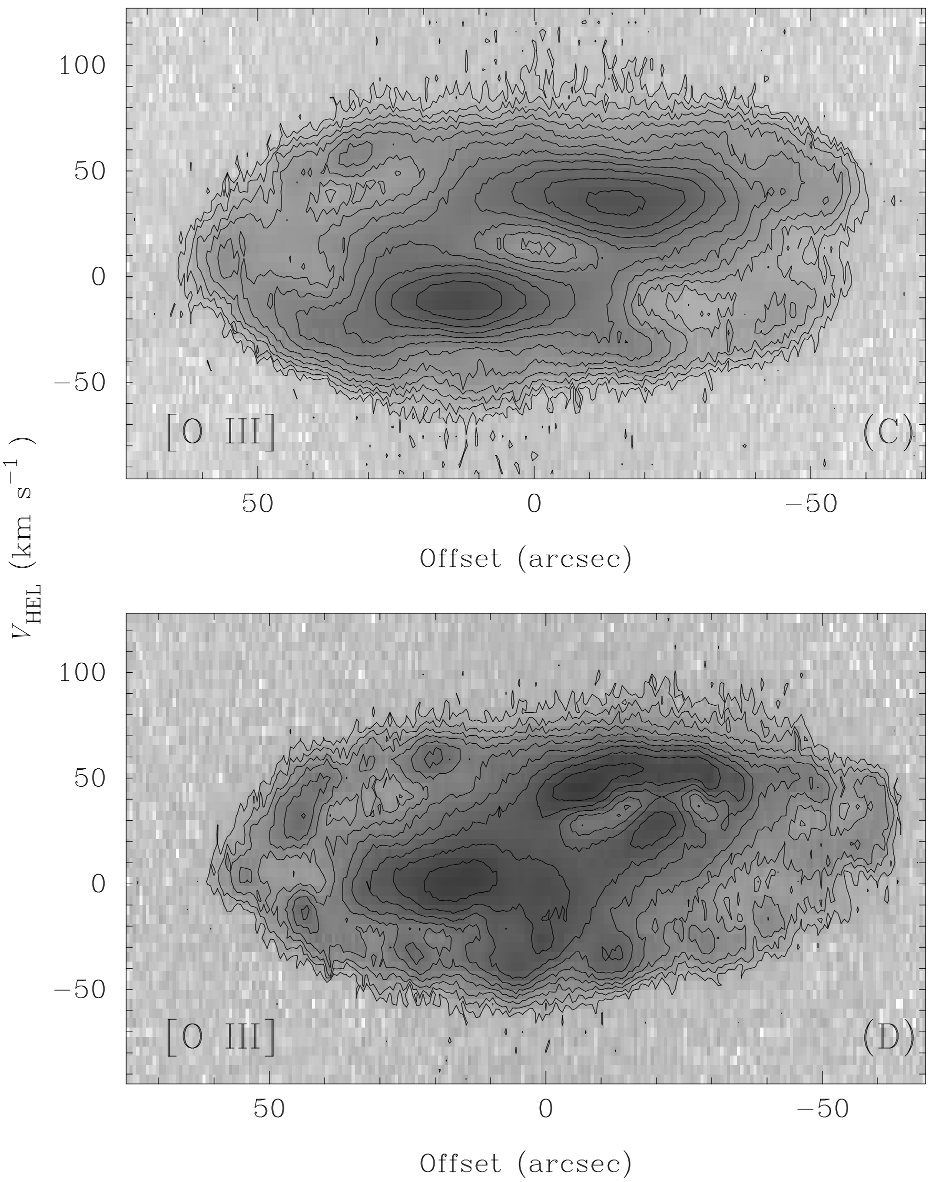

Figure 6. As Fig. 4 but for the position–velocity arrays of the [O III] λ5007 line profiles for slit positions C and D.

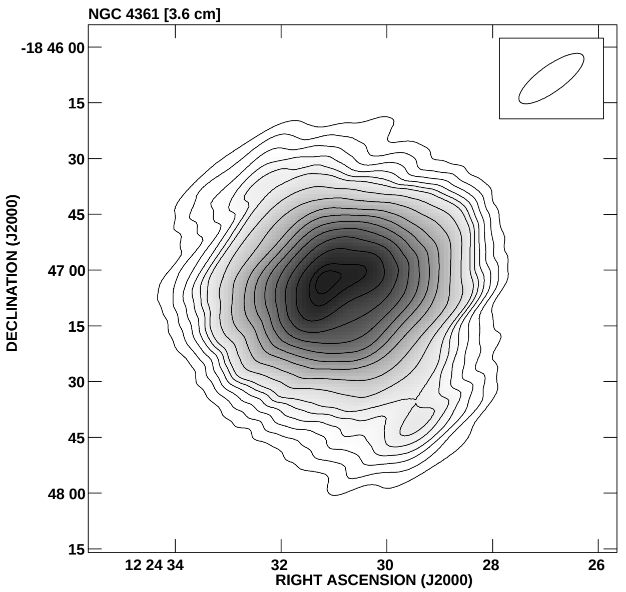

Figure 7. Grey-scale with contour plot λ3.6-cm continuum map of NGC 4361. Contour levels are 6, 9, 12, 15, 18, 21, 28, 38, 50, 60, 70, 80, 90, 100, 108, 110 times 80 μJy beam^{-1}, the rms noise in the map. The half-power contour beam (21.1 × 7.0 arcsec^2, PA − 54°) is also shown.

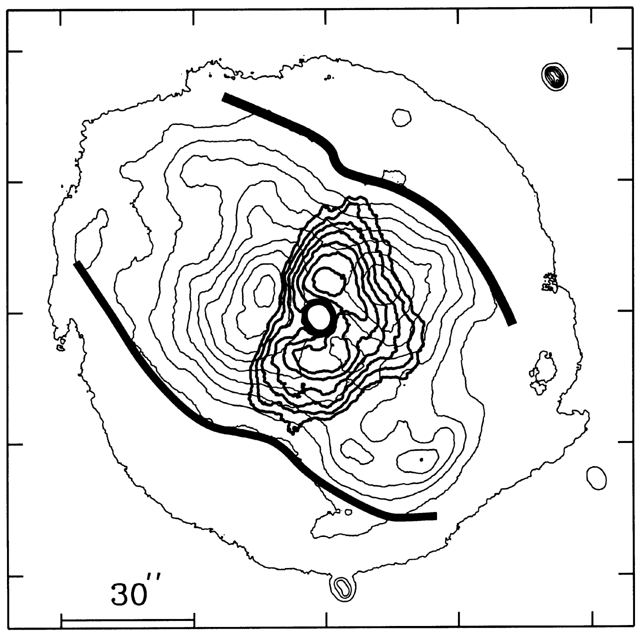

Figure 8. Schematic representation of the main configurations in NGC 4361. Contours derived from the [O III] image are drawn in thin lines. Thick lines trace the lowest values of the [O III]/Hα image ratio; the ratio decreases towards the centre, being minimum in two regions separated by ≃ 18 arcsec and oriented at PA ≃ −20°. Bold lines delineate the resultant bipolar configuration.

$V_{\rm HEL} \simeq 20$–$30\,{\rm km\,s^{-1}}$ at the western side. The asymmetry of this expansion is also particularly apparent in slit position A, top panel in Fig. 5. Moreover, the systemic heliocentric radial velocity, $V_{\rm sys} \simeq 12\,{\rm km\,s^{-1}}$, defined here by the middle point between the bright central expanding condensations, does not coincide with the terminal radial velocities mentioned above. This indicates that either the halo is not an expanding spherical volume (but rather an ellipsoid whose main axis presents a substantial tilt with respect to the line of sight – e.g. Frank & Mellema 1994), or that the expansion of the halo is being distorted by an inner, non-radially expanding flow, as in the case of NGC 6572, in which a bipolar collimated outflow has been recently shown by Miranda et al. (1999) to be interacting with its surrounding shell.

3.3.2 *The inner shell*

The emission maxima in the bright central condensations show expansion velocities for Hα, He II λ6560 and [O III] λ5007 of 17, 17 and $23\,{\rm km\,s^{-1}}$, respectively (top panels in Figs 4 and 6).

All the main velocity components within all the profiles are seen to be redshifted if they are located west of centre and correspondingly blueshifted on the eastern side. However, their structure cannot be interpreted as a result of a simple radial expansion.

A chain of relatively bright [O III] knots is seen in slit positions B, C and D (Fig. 5, bottom panel, and Fig. 6) to surround the halo on its inner side. A close inspection of these velocity components reveals a certain degree of point-symmetry within each profile, i.e. those located on the west side of the profile and with positive systemic radial velocities have their corresponding counterparts on the opposite side at negative systemic radial velocities.

Morphological structures are usually seen replicated in spatially-resolved long-slit spectra and it is noted that the overall structure of these line profiles resembles that expected from a loose bipolar outflow (see e.g. Bryce et al. 1996). This is particularly evident in the main velocity components of the line profile for slit C (Fig. 6, upper panel), which crosses the projected nebular centre, but it is also apparent in the line profiles B and D (Figs 5 and 6, lower panels) located above and below position C, where the central velocity components have bipolar looking structures that seem here tilted. The detailed spatially-resolved kinematics of NGC 4361 therefore indicates the presence of an inner bipolar structure with its north-eastern lobe predominantly blueshifted and the south-western one redshifted (slits B and D), and with slit C running across the projected central portion of the tilted bipolar configuration.

3.3.3 *The bipolar outflow*

The location of the bright [O III] knots in the nebular centre are puzzling and hamper a clear visualization of the bipolar structure. In order to clarify their true relevance within the bipolar interpretation, the [O III]/Hα image ratio has been derived.

Fig. 8 presents a contour plot of the nebula from the [O III] image drawn using thin lines. Overplotted in thick lines are the contours from the lowest values of the [O III]/Hα image ratio, in which Hα dominates the central region over [O III]. The ratio decreases towards the centre with the Hα emission dominating in a distinct central elongated band. Minimum ratio values (highest Hα) are found in two regions separated by ≃ 18 arcsec and oriented along PA −20°. The [O III]/Hα ratio provides mainly a diagnostic on the local excitation or ionization conditions. Close to the hot nucleus of NGC 4361, oxygen may be ionized to higher stages than O^{2+}, contributing to the low [O III]/Hα ratio values derived near the core. However, this ratio is also sensitive to temperature variations that in turn introduce a moderate density dependence (cf. Corradi et al. 1996). The λ3.6-cm radio continuum map (Fig. 3) indicates higher densities in the central region. Under these considerations, the orientation of the localized, elongated structure defined by [O III]/Hα suggests the presence of an equatorial plane perpendicular to the bipolar outflow that would fit the kinematic interpretation. Thicker (bold) lines in Fig. 8 outline the resultant bipolar structure, that can be now clearly recognized.

It is interesting to notice now in Figs 1, 2 and 3 that the bipolar outflow, whose projected main axis lies at PA$\approx$60° seems to interact with the borders of the outer shell, distorting the circular appearance of the halo along this direction and lending weight to the alternative interpretation of a non-radial expansion from the inner regions, as discussed in Section 3.3.1. In this case, the chain of bright [O III] knots that surround the halo on its inner side and display a certain degree of point-symmetry may be interpreted as contact points of the bipolar outflow with the outer shell. For this interaction to happen, the bipolar outflow must then be able to catch up with the fast expanding outer shell.

The maximum observed radial expansion velocity in the bipolar structures is 55 km s^{-1} (≈ -40 and $+70$ km s^{-1}). To reach and start overrunning the fast expanding halo within a reasonable time, the deprojected velocity of the bipolar outflow must then be greater than the observed 70 km s^{-1} expansion velocities of the outer shell. For a distance to NGC 4361 of 1.2 kpc, the 55-arcsec radius of the halo corresponds to 0.32 pc and the kinematic age for the halo would be 4.5×10^3 yr. Considering that the bipolar outflow must be younger than the halo, the following relation must hold:

$$\tau_\mathrm{b} = R/V_\mathrm{p} = (X/V)\tan\alpha < 4500\,\mathrm{yr},$$

where τ_b is the kinematic age of the bipolar outflow; $X = 68$ arcsec is the length of the NE lobe as measured from Fig. 2; $V = 55$ km s^{-1} is the measured radial expansion velocity of the bipolar lobes; α is the angle of the bipolar flow with respect to the plane of the sky; $R = X/\cos\alpha$ is the deprojected length of the NE lobe and $V_\mathrm{p} = V/\sin\alpha$ is the expansion velocity of the bipolar flow along the polar axis.

This implies that $\tan\alpha < 4500V/X$, deriving an upper limit for $\alpha < 33°$ and a lower limit for $V_\mathrm{p} > 100$ km s^{-1}. For values of $20° \leqslant \alpha \leqslant 30°$ the kinematic age for the bipolar outflow ranges from 2500 to 4000 yr, considering constant velocities. These simple estimates indicate that the onset of the bipolar outflow occurred between 500 to 2000 yr after the slow wind at the end of the AGB phase, from which the halo must have been formed. These times are characteristic of normal type PNe, but seem short for a very-low-mass progenitor, for which the evolutionary processes are expected to be much slower according to current models. In fact, Méndez et al. (1988) have derived for NGC 4361 a core mass $M_\mathrm{core} = 0.55 \pm 0.01\,\mathrm{M}_\odot$, which would correspond to a progenitor of $\leqslant \mathrm{M}_\odot$, and a current effective temperature $T_\mathrm{eff} = 82\,000 \pm 5000$ K. Isochrones for a core with these characteristics imply evolutionary times after the AGB phase greater than 10^4 yr (Vassiliadis & Wood 1994; Blocker 1995), which are clearly in conflict with the kinematic ages derived above. A likely explanation for this is that the current high expansion velocity of the halo is the result of a progressive acceleration through its evolution and therefore its kinematic age is subestimated. Consequently, the halo in NGC 4361 must actually be older. In this case, larger values for the angle α and lower polar velocities V_p would be allowed. Indications of accelerated expansions of the nebular shell in the early stages of evolution have been pointed out before by Dopita & Meatheringham (1990) for Magellanic PNe.

The highly filamentary structure of NGC 4361, as shown in Fig. 2, may also be linked to the evolutionary process of the hot bubble in this nebula. According to Mellema & Frank (1995), after full ionization of the 'slow' wind, as in this case, the hot bubble becomes very sensitive to disturbances such as those produced by the secondary fast wind and the effects of shocks, and becomes turbulence-prone.

Previous investigators have pointed out the presence of temperature variations in this nebula. From the nebular Balmer jump (BJ) Barker (1978) and Liu & Danziger (1993) obtain $T_\mathrm{e}(\mathrm{BJ}) = 16\,400$ and $13\,000$ K, respectively, with large associated uncertainties. Recently, Liu (1998) has derived from long-slit observations the electron temperature from the [O III] lines; his slit is oriented E–W and 10 arcsec N from the core. The derived T_e[O III] is $\simeq 18\,000$ K for the central ±15 arcsec region, and this value tends to increase outwards reaching 20 000 K, where the 'inner shell and the fainter outer halo meet' (compare Figs 1 and 4 in Liu 1998 with Fig. 8 in this paper). In view of these temperature variations, Liu (1998) has suggested the possibility of shocks as an additional source of heating in this nebula.

It is thus of interest to consider the possible effects on the structure of the nebula for a 100 km s^{-1} inner bipolar outflow over the outer shell that advances at a speed of 70 km s^{-1}. In this case, the faster component will encounter the slower one with a relative (upstream) velocity $V_0 = 30$ km s^{-1} at the polar regions. Along the inner regions, the relative velocities will be lower since only the normal velocity component of the outflow with respect to the 'walls' of the bipolar cavity would play a role. The isothermal sound speed in the high excitation medium of NGC 4361 is $\approx$17 km s^{-1}. Considering these limits for the relative velocities (17–30 km s^{-1}), the Rankine–Hugoniot jump conditions yield in these cases shock velocities in the range $V_s \simeq 32$–46 km s^{-1}, and temperature increments in the regions behind the shock of 6000 to 18 000 K with respect to the pre-shock [O III] temperature. The compression in the density ratio, ρ_1/ρ_0, for these weak shocks amounts to factors of only 2.13 to 2.83 for the values considered. The amount of additional specific internal energy deposited by these shocks, $E_\mathrm{i} = \frac{3}{2}nkT$, is in the range ≈ 1.28–2.53×10^{-8} ergs cm^{-3} and the associated specific kinetic energy, $E_\mathrm{k} = \frac{1}{2}V_1^2$ (where V_1 is the downstream velocity), takes values in the range 1.27–1.52×10^{-8} erg cm^{-3}, respectively (cf. Dyson & Williams 1980). Adopting a value for the radiative cooling $\Lambda = 10^{-22}$ erg cm^3 s^{-1}, for the conditions of interest here (Sutherland & Dopita 1993), the corresponding characteristic cooling time would be of the order of 0.6 yr. This is much shorter than typical recombination times and, although the cooling length in this situation is only of the order of 10^{14} cm, with the bipolar outflow spreading the shock over a large nebular region, time-dependent cooling effects may become important (cf. Shapiro & Moore 1976) and possibly relevant for the analysis of ionic abundances, as the one relating to C in this nebula (Liu 1998; TPPP).

It should be noted that the conditions assumed in this analysis have been adopted from one of the likely, conservative, situations derived in the discussion given previously. However, the detection of soft X-ray emission by *ROSAT* (Kreysing et al. 1992) suggests that stronger shocks may be involved in the dynamics of this nebula. Nevertheless, under the assumed conditions and simple calculations presented above it is shown that the effects of relatively weak shocks can provide an additional source of heating to the thermal structure of NGC 4361.

4 CONCLUSIONS

Ground-based, optical imagery, long-slit spatially-resolved echelle spectra and VLA-DnC λ3.6-cm continuum observations have been presented for NGC 4361, a type IV Population II PN. The rms electron density and dimensions derived from the radio continuum data and the electron density from forbidden lines derived by Liu (1998) have allowed an independent confirmation of the large volume filling factor and corresponding low mass of the nebular envelope in this object, yielding a value of $M(\mathrm{H\,II}) = 0.07\,\mathrm{M}_\odot$

The detailed analysis of the morphology and kinematics of NGC 4361 has disclosed the presence of a bipolar outflow in this object, an unexpected kinematics for a Population II PN since bipolar outflows are believed to be related mainly to Population I type I PNe (Peimbert & Torres Peimbert 1983; Corradi & Schwarz 1995).

The global structure of NGC 4361 is described by a fast, expanding halo that is being overrun by an even faster central bipolar outflow. The interaction of this non-radial outflow with the halo has already produced notorious signs of deformation in the latter.

The kinematic age (4.5×10^3 yr) derived for the halo under the assumption of a constant expansion velocity is found to be in conflict with the evolutionary age expected for the low-mass core in NGC 4361 ($>10^4$ yr). A larger age for the halo could be explained in terms of an accelerated expansion during the early stages of development. The fast wind has still been able to develop an axisymmetrical outflow before full erosion of the equatorial material, whose remnant is now weakening but still apparent, as has been revealed in the [O III]/Hα image ratio.

It has been shown that shocks can provide an additional source of heating in this nebula, which can partially account for the temperature variations observed. Time-dependent cooling effects in this case may be relevant to understanding the discrepant C ionic abundances that have been previously found in this object.

The fact that a presumably slowly-evolving Population II PN with a low-mass progenitor is still able to generate a bipolar outflow raises new questions on the conditions for the onset of bipolarity that will have to be addressed by the models. Clearly, a detailed inspection of the other known PNe that belong to the thick disc or halo population is called for to investigate weather NGC 4361 is a peculiar case or not. When the available HST archive public images were inspected, no apparent signs of binarity were found.

ACKNOWLEDGMENTS

This work has been partially supported by the Programa de Cooperación Científica con Iberoamerica. RV is in grateful receipt of a graduate scholarship from the AECI (Spain) and complementary support from DGAPA-UNAM (Mexico). JAL acknowledges continuous support from DGAPA-UNAM (Mexico) and the Junta de Andalucía for a travel grant to the IAA, where part of this paper was written. LFM, JMT and RV are supported in part by DGICYT Grant PB95-0066 and by Junta de Andalucía (Spain). JMT acknowledges the hospitality offered by the Departament de Fisica of the Universitat de les Illes Balears (UIB) and the Instituto Mediterráneo de Estudios Avanzados (CSIC-UIB) (Spain) during the preparation of this paper. The authors also thank the staff of the San Pedro Mártir Observatory for their excellent assistance during these observations. RV gratefully acknowledges several discussions with H. Aceves during the course of this work.

REFERENCES

Barker T., 1978, ApJ, 219, 914
Blocker T., 1995, A&A, 299, 755
Bryce M., Meaburn J., Walsh J., Clegg R. E. S., 1992, MNRAS, 254, 477
Bryce M., Mellema G., Clayton C. A., Meaburn J., Balick B., Lopez J. A., 1996, A&A, 307, 253
Chu Y.-H., Jacoby G. H., 1987, in Kwok S., Pottasch S. T., eds, Late Stages of Stellar Evolution. Reidel, Dordrecht, p. 351
Chu Y. H., Arendt R., Jacoby G. H., 1987, ApJS, 64, 529
Corradi R. L. M., Schwarz H. E., 1995, A&A, 293, 871
Corradi R. L. M., Manso R., Mampaso A., Schwarz H. E., 1996, A&A, 313, 913
Dopita M. A., Meatheringham S. J., 1990, ApJ, 357, 140
Dyson J. E., Williams D. A., 1980, Physics of the Interstellar Medium, Wiley, New York
Frank A., Mellema G., 1994, ApJ, 430, 800
Kreysing H. C., Diesch C., Zweigle J., Staubert R., Grewing M., Hasinger G., 1992, A&A, 264, 623
Liu X. W., 1998, MNRAS, 295, 699
Liu X. W., Danziger I. J., 1993, MNRAS, 263, 256
Meaburn J., Blundell B., Carling R., Gregory D. E., Keir D. F., Wynne C. G., 1984, MNRAS, 210, 463
Meatheringham S. J., Wood P. R., Faulkner D. J., 1988, ApJ, 334, 862
Mellema G., Frank A., 1995, MNRAS, 273, 401
Méndez R. H., Kudritzki R. P., Herrero A., Husfeld D., Groth H. G., 1988, A&A, 190, 113
Mezger P. G., Henderson A. P., 1967, ApJ, 147, 471
Miranda L. F., Vázquez R., Corradi R. L. M., Guerrero M. A., López J. A., Torrelles J. M., 1999, ApJ, 520, 714
Peimbert M., 1990, Rep. Prog. Phys., 53, 1559
Peimbert M., Torres-Peimbert S., 1983, in Flower D. R., ed., Proc. IAU Symp. 103, Planetary Nebulae. Reidel, Dordrecht, p. 233
Schwarz H. E., Corradi R. L. M., Melnick J., 1992, A&AS, 96, 23
Shapiro P. R., Moore R. T., 1976, ApJ, 207, 460
Sutherland R. S., Dopita M. A., 1993, ApJS, 88, 253
Torres-Peimbert S., Peimbert M., Peña, M., 1990, A&A, 233, 540 (TPPP)
Vassiliadis E., Wood P. R., 1994, ApJS, 92, 125

This paper has been typeset from a TEX/LATEX file prepared by the author.